Calorimetric analysis of Portevin-Le Chatelier bands under equibiaxial loading conditions in Al–Mg alloys: Kinematics and mechanical dissipation

Jean-Benoit Le Cam, Eric Robin, Lionel Leotoing, Dominique Guines

Calorimetric analysis of Portevin-Le Chatelier bands under equibiaxial loading conditions in Al-Mg alloys: kinematics and mechanical dissipation

Jean-Benoît Le Cam [a,1], Eric Robin [a], Lionel Leotoing [b], Dominique Guines [b]

[a] *Université de Rennes 1, Institut de Physique UMR 6251 CNRS/Université de Rennes 1, Campus de Beaulieu, Bât. 10B, 35042 Rennes Cedex, France*

[b] *LGCGM, INSA, UEB, 20 avenue des Buttes de Coesmes, 35708 Rennes Cedex, France*

Abstract

This paper investigates the thermomechanical behavior of Al-Mg alloys submitted to equibiaxial loading until failure. More particularly, the study aims to characterize calorimetric signature accompanying the formation and propagation of Portevin-Le Chatelier (PLC) bands induced by such a loading condition. Digital Image Correlation (DIC) and infrared thermography (IRT) on both sides of a cruciform shaped specimen were performed in order to characterize full kinematic and thermal fields on the specimen surface. Heat source field was reconstructed from the temperature field and the heat diffusion equation. The heat source map enables us to visualize spatio-temporal gradients in the calorimetric response of the material and to investigate the kinematics of PLC bands induced by equibiaxial tensile loading. At the

specimen centre, the heat source exhibits jumps that fit with jumps of temperature and equivalent deformation rate. Until a 30% equivalent strain rate is reached, these jumps are due to repeatable PLC band propagation in the two perpendicular loading directions. In certain cases, heat source maps may be seen as mechanical dissipation maps.

Key words: Portevin-Le Chatelier effect, Aluminum alloy, equibiaxial tension test, infrared thermography, heat source reconstruction

1 Introduction

Plastic instabilities take place in numerous materials such as low carbon steels, mild steels and Al-Mg alloys (1). They reduce material ductility and induce surface roughness, which are parameters of crucial significance in the field of sheet metal forming. The Portevin-Le Chatelier (PLC) effect is such a plastic instability and is one of the macroscopic manifestations of dynamic strain aging (DSA), *i.e.* interactions between mobile dislocations and diffusing solute atoms (2; 3). From a mechanical point of view, it corresponds to an irregular plastic flow and propagation of high-strain bands in the material (4; 5; 6). Numerous studies have been dedicated to the characterization of the motion and morphology of the bands (7; 8; 9). The occurrence of PLC bands depends on several mechanical parameters such as strain level, strain rate and temperature. Three types of PLC bands (A, B and C) are reported in the literature (10; 11; 12; 13; 14). They are mainly governed by the strain rate and appear successively (from A to C) when the strain rate is decreased. Generally, PLC effects are investigated under uniaxial tension. Very few studies

[1] Corresponding author eric.robin@univ-rennes1.fr Fax : (+33) 223 236 111

focus on the occurrence of PLC under compression (15). A Single study was carried out in another monotonic strain path (the simple shear, (16)). Concerning the type of material used, Al-Mg alloys are some of the most studied systems (17; 18; 19; 20; 21), typically the AA5000 series (5086, 5182 or 5754 for instance). To our knowledge, no study has been reported in the literature on PLC effects in Al-Mg alloys under equibiaxial tension, while most metal forming operations are carried out under these loading conditions.

Furthermore, plastic deformation in metals leads to the dissipation of the main part of the mechanical energy into heat. This mechanical dissipation (or intrinsic dissipation) results in an increase of the material temperature. It is therefore relevant to investigate PLC effects in a complementary manner by measuring temperature variation at the surface of the material. Several studies in this field have been reported in the literature (22; 16; 23; 24; 25). In most studies, infrared cameras are used to measure the temperature field at the surface of the specimen. During mechanical loading, materials produce or absorb heat due to reversible processes (thermoelasticity (26), rubber elasticity (27), latent heat of solid-solid phase transition (28)) and irreversible processes (viscosity (29), plasticity (30), damage (31; 32)), depending on the type of material. Numerous studies previously carried out by Chrysochoos et al. have shown that heat sources produced by the material itself are more relevant than temperatures for analyzing such phenomena ((33; 34; 35; 36)). The main reason is that the temperature field is influenced by heat conduction as well as heat exchanges with the ambient air and the grips of the testing machine. To our best knowledge, only studies (37) and (38) provide heat source distributions induced by PLC effects in a metallic material. The characterization tests were performed under uniaxial tensile loading conditions.

This paper investigates the PLC effects in Al-Mg alloy sheet under equibiaxial loading conditions by means of IR thermography measurements and heat source reconstruction. Several test configurations can be used to induce this equibiaxial stress state in a metal sheet. The best known is the so-called bulge test (39; 40). In this case, the specimen surface does not remain flat during its deformation, which makes thermal field measurements by using an infrared camera impossible. To counter this, tests were performed with a biaxial testing machine described in (41). The device is a servo-hydraulic testing machine composed of four independent dynamic actuators enabling biaxial tensile tests on cruciform specimens. Kinematics and thermal field measurements were performed on both sides of the specimen. Heat sources produced or absorbed by the material itself during deformation are deducted from temperature field measurements by using the heat diffusion equation. The heat source map enables us to visualize spatio-temporal gradients in the calorimetric response and to investigate the kinematics of PLC bands induced by equibiaxial tensile loading. In certain cases precisely detailed in the paper, the heat source map gives the mechanical dissipation field.

The paper is structured as follows. Section 2 presents the material and specimen geometry, the experimental device and the full field measurement techniques used. Section 3 recalls how heat sources are reconstructed from thermal field measurements in case of bi-dimensional problems. Section 4 gives the results obtained. The kinematics of PLC bands are discussed in relation to the heat sources distribution during deformation. Mechanical dissipation associated with the deformation processes are mapped. Concluding remarks close the paper. A video for which a link is provided in Appendix A illustrates the main results of this study.

2 Experimental setup

2.1 Material and geometry

Due to their high strength to weight ratio, corrosion resistance, good formability and weldability, aluminum alloys in the AA5000 series are widely used in the manufacturing of industrial products. The material reviewed here is the aluminium alloy AA5086-H111. It is an Al-Mg alloy with an average magnesium weight ratio of 4%. Numerous cruciform shaped specimens have already been designed to characterize the diverse mechanical behaviour of metallic sheets: yield locus (42), hardening (43), forming limits (41). A direct control of the strain path at the specimen centre is ensured thanks to the displacement control of the independent actuators acting on the four arms of the specimen. In order to reach high strain levels in the central zone of the specimen, a dedicated cruciform shape must be designed. From finite element simulations, a sample form, illustrated in Figure 1, has been optimized and submitted by the present authors (41). To concentrate strains in the central zone, strain localisation at the junction of two arms is reduced by a radius and by longitudinal slots which decrease the transversal stiffness of the arms. A progressive thickness reduction in the central zone is adopted. The central region of the specimen is manufactured by using a computer numerical control (CNC) lathe.

2.2 Loading conditions

The proposed experimental device is a servo-hydraulic testing machine provided with four independent dynamic actuators, permitting biaxial tensile

tests on cruciform specimens along two perpendicular axes. The overview of the experimental set-up is given in Figure 2(a). For each actuator, the loading capacity is $50kN$ and the maximum velocity can reach up to $2m.s^{-1}$. The strain path (linear or non linear) during the test can be directly controlled by the actuator motion. The results presented in this work are obtained under an equibiaxial strain state, with the same velocity of $1mm.s^{-1}$ for both axes.

2.3 Kinematic field measurement

Images of the gauge area of the cruciform specimen were recorded with a Fastcam Ultima APX-RS digital camera. As shown in Figure 2(a), the camera is placed perpendicularly to the surface observed. Images are obtained by using an optical mirror. A frequency of 250 frames per second is set. Considering the image size and the camera position, a resolution of 0.054 $mm/pixel$ is obtained. The DIC software CORRELA 2D was used to compute the in-plane strain field. Major and minor strains are calculated ($27points \times 27points$) on a square area (approximately $16mm \times 16mm$), as shown in Figure 2(b). Equivalent strain is calculated as follows:

$$\bar{\epsilon} = \sqrt{\frac{2}{3}\sum_{i,j}\epsilon_{ij}^2} \tag{1}$$

where ϵ_{ij} are the components of the strain tensor.

2.4 Temperature field measurement

Temperature field measurements were performed using a FLIR X6540sc InSb infrared camera, which features a focal plane array of 640x512 pixels and de-

tectors with a wavelength range of 1.5-5.1 μm and a pitch of 15 μm. Integration time was equal to 1000 μs. The acquisition frequency was set at 250 frames per second. The thermal resolution, namely the noise-equivalent temperature difference, was equal to 20 mK at 25°C. The camera detector calibration was performed with a black body using a Non-Uniformity Correction (NUC) procedure. The temperature field was extracted from the IR image by using the infrared provider software and was then processed by means of Matlab software. Temperature variation fields were obtained by subtracting the initial temperature field (before applying mechanical loading) from the current one. In practice, the initial temperature field is obtained by averaging several images, in order to reduce the noise effect. The spatial resolution, corresponding to the pixel size on the measurement plane, was equal to 0.206 $mm/pixel$. A thin, opaque and uniform black paint was sprayed on the specimen surface to obtain a thermal emissivity close to one.

2.5 Bi-dimensional heat source reconstruction from temperature field measurement

This section briefly recalls the thermomechanical framework that is usually used to calculate heat sources (44). The thermodynamic process is considered as a quasi-static phenomenon. The state of any material volume element is defined by N state variables: temperature T, one of the strain tensors denoted E and some internal variables $V_1, V_2, \ldots, V_{N-2}$ such as plastic strain or volume fractions of some phases. The specific free energy potential is denoted $\Psi(T, E, V_k)$. Considering the first and second principles of thermodynamics and assuming that Fourier's law is used to model heat conduction, the heat

diffusion equation can be written as follows:

$$\rho\, C_{E,V_k}\, \dot{T} \;-\; \mathrm{div}\,(K\ \mathrm{grad}\ T) \;-\; r \;=\; \underbrace{d_1 \;+\; \rho T \frac{\partial^2 \Psi}{\partial T \partial E}\, \dot{E} \;+\; \rho T \frac{\partial^2 \Psi}{\partial T \partial V_k}\, \dot{V_k}}_{s} \quad (2)$$

where ρ is the density, C_{E,V_k} is the specific heat at constant E and V_k, K is the thermal conductivity tensor and r is the external heat source. The right-hand side of the equation (2) represents the heat sources s produced by the material itself. It can be split into different terms:

- *mechanical dissipation* d_1 (or *intrinsic dissipation*). This positive quantity corresponds to the heat production due to some mechanical irreversibilities such as internal friction;
- *thermomechanical couplings*: they correspond to the couplings between the temperature and the other state variables. The coupling between temperature and strain $\rho T \frac{\partial^2 \Psi}{\partial T \partial E}\, \dot{E}$ is the *thermoelastic coupling* (34; 45).

Assuming that the heat conduction is isotropic, integrating the heat diffusion equation (Equation 2) over the specimen thickness and using the temperature variation leads to the following bidimensional formulation of the heat diffusion equation (46):

$$\rho\, C_{E,V_k}\, \dot{T} \;-\; k\, \Delta\, T \;-\; r \;= s \quad (3)$$

where Δ is the laplacian operator and k the conductivity coefficient. Let us now consider a flat specimen. (x, y, z) is a cartesian coordinate system such that the x-direction is the main direction of the specimen and the z-direction is perpendicular to the mid-plane. It should be noted that the maximum thickness must be weighed against the thermal conductivity of the material to ensure a homogeneous temperature over the entire thickness. On the other hand, the

temperature gradient $\partial T/\partial z$ is not constant near the front and back sides of the specimen because of heat exchanges with ambient air (46). Averaging Equation (3) through the thickness of the specimen leads to:

$$\rho\ C_{E,V_k}\ \dot{\bar{T}}\ -\ k\ \left(\frac{\partial^2 \bar{T}}{\partial x^2}+\frac{\partial^2 \bar{T}}{\partial y^2}\right)-\frac{1}{e}\ k\left[\frac{\partial T}{\partial z}\right]_{-e/2}^{e/2}-\ r\ =s \tag{4}$$

where e is the specimen thickness and $\bar{T}$ is the mean through-thickness temperature. The material parameters ρ, C_{E,V_k}, k, the external heat sources r and the heat sources s produced by the material itself are also assumed to be constant through the thickness of the specimen. By using temperature variation θ instead of temperature and by considering that the external heat sources r and the material parameters ρ, C_{E,V_k} k are constant during the test, the 2D-version of the heat diffusion equation is expressed as:

$$\rho\ C_{E,V_k}\ \left(\dot{\theta}+\frac{\theta+T_0-T_{\text{amb}}}{\tau}\right)-k\ \Delta_{2D}\theta\ =s \tag{5}$$

where Δ_{2D} is the two-dimensional Laplace operator in the (x, y) plane. τ is the time constant, which is considered as a time constant characterizing the heat exchange with ambient air. This time constant can be identified from a return to ambiant temperature.

Remark #1: in practice, temperature fields are captured by an IR camera. To estimate heat sources s produced by the material, the procedure consists in calculating the left-hand side of the equation (5) by processing the bi-dimensional temperature fields.

Remark #2: thermal data are noisy and this noise is amplified by differentiation, when calculating the corresponding heat sources. This is all the more true as first and second derivatives must be calculated.This is why temperature

field evolution is filtered beforehand by a 7x7x7 average spatio-temporal filter. Then, the temperature variation field is processed.

Remark #3: the relative smallness of the thermal dilatability of Mg-Al alloys suggests that the heat source due to the thermoelastic couplings becomes rapidly negligible when compared with the mechanical dissipation developed during the elastoplastic transformation. Moreover, small temperature variations induced by the deformation process are assumed to have no influence on the hardening state. As a consequence, the heat sources related to the coupling terms between temperature and the other internal variables can also be neglected. These assumptions have previously been adopted in (46). These assumptions lead to consider heat source map and once plasticity starts, lead us to consider the heat source map as mechanical dissipation map.

3 Results

3.1 Mechanical response

Figure 3 shows that force variation obtained in the two perpendicular loading directions. The curves show that forces evolve in a similar manner in both directions, which means that the test was conducted under quasi-perfect equibiaxial loading conditions. The slight difference is due to material anisotropy. The first part of the curves ($t \in [1.75; 2.2]$) corresponds to the elastic deformation of the cruciform specimen. In the second part of the curve ($t > 2.2\ s$), plastic deformation starts at a corresponding force approximately equal to 2400 N. In the plastic domain, the zoom in on the curves shows that force profiles exhibit slight fluctuations. Under tensile loading conditions, such fluc-

tuations are the signature of type A PLC bands (14).

3.2 Thermal response at the specimen centre

Figure 4 gives the temperature variations and equivalent strain at the centre of the cruciform specimen versus time. The temperature is obtained by averaging temperatures over a 5x5 pixel zone at the specimen centre (approximately $1mm^2$). Equivalent strain is issued from DIC calculation in a zone of 64x64 pixels (approximately $9mm^2$).

At the very beginning of the test, strain increase leads to temperature decrease. This is typically observed in purely thermoelastic response of materials such as metallic ones: to deform, the material needs energy and absorbs heat. From t=2.3s on, temperature increases. Mechanical dissipation due to plasticity is produced and is of a first order compared to the thermoelastic coupling. Then, in the plastic domain, equivalent strain exhibits strong variations. Equivalent strain rate alternates between low (but always positive) and high values, which forms steps in the plastic domain. When equivalent strain rate value is high, temperature strongly increases. This is the signature of PLC bands formation and propagation. When equivalent strain rate is low, temperature decreases. Two phenomena could explain this temperature decrease. The first phenomenon corresponds to heat diffusion by conduction and convection. In this case, the higher the temperature reached after the high increase in equivalent strain should induce a higher temperature drop. This phenomenon can be observed by comparing the slopes of the dotted lines #2 to 5, given by the slope (#1) of the thermal response in the purely elastic domain ($(t \in [1.75; 2.2])$), with the slopes of the temperature drop. This phe-

nomenon was invoked by Bernard et al. in (25). The second phenomenon is thermoelasticity. Certainly, after the PLC band passage and the corresponding jump in equivalent strain and temperature, the material should deform purely elastically and therefore absorb heat. This was previously observed under uniaxial loading conditions by using quantitative calorimetry in (38). To assess the relative contribution of heat diffusion and thermoelastic coupling to temperature drops, a calorimetric analysis has been carried out. It is presented in the next section.

3.3 Calorimetric response at the specimen centre

Figure 5 presents the evolution of temperature and heat sources versus time. Heat sources are deduced from temperature variation by applying the bidirectional formulation of the heat diffusion equation given in Equation 5. The time constant has been identified from a return to ambient temperature and is equal to 30 s at the specimen centre. The density and specific heat are respectively equal to 2650 kg/m^3 and 970 $J/(K.kg)$. In this diagram, the blue color zone corresponds to the thermoelastic effect: the material absorbs heat and temperature decreases. The red color zones correspond to temperature jumps. As shown in this figure, temperature jumps are due to jumps in heat source. From $t = 2.2$ s on, the material continues absorbing heat but at a lower rate, since mechanical dissipation due to plasticity occurs. From $t = 2.3$ s on, heat produced due to plasticity is superior to heat absorbed due to thermoelasticity, and the heat source becomes positive. As a consequence, the temperature starts to increase. Subsequently, each jump in the equivalent strain induces a strong heat production and a jump in temperature. In terms of heat sources,

the maximum value reached during the jumps increases monotonically from 5.10^6W/m3 to 3.10^7 W/m3 and more before failure.

Between two strain jumps, equivalent strain rate is lower (but always positive) and corresponding average heat sources mostly negative (see Figure 6). This proves that after PLC band passage, the material mainly deforms elastically. The fact that the higher the temperature reached after a jump, the higher the slope value (see Figure 4), shows that heat diffusion also occurs. After each equivalent strain rate jump, the equivalent strain rate is constant and positive. Its value increases after each successive jump.

To fully assess the relative contribution of heat diffusion, Figure 7 gives the evolution of heat conduction, heat convection and total heat sources during the test. Total heat source is related to left-hand axis, heat conduction and convection to right-hand axis. Compared to the total heat source, heat diffusion due to conduction is close to zero and heat diffusion due to convection is about two orders of magnitude less than the total heat sources. For each temperature drop (from # 1 to 5 in Figure 4), the ratio of heat diffusion over total heat source has been calculated:

$$\frac{\mid \rho \; C_{E,V_k} \; \left(\frac{\theta+T_0-T_{amb}}{\tau}\right) - k(\Delta_{2D}\theta) \mid}{\mid \rho \; C_{E,V_k} \; \left(\dot{\theta} + \frac{\theta+T_0-T_{amb}}{\tau}\right) - k(\Delta_{2D}\theta) \mid} \times 100 \tag{6}$$

Results are reported in Table 1 and show that the maximum contribution of heat diffusion reaches less than 1% of the total heat source. These results prove that temperature drops after PLC band passage are mainly due to thermoelasticity. In the following, heat sources are mapped in order to investigate the kinematics of PLC bands.

3.4 Bidimensional heat source reconstruction

3.4.1 PLC band kinematics

The kinematics of PLC bands is usually investigated under uniaxial loading conditions by using full field kinematic measurements. It is also investigated using quantitative calorimetry obtained by temperature field measurement, since these bands have a specific calorimetric signature (38). To our knowledge, this is the first study of PLC band kinematics under equibiaxial loading condition by means of quantitative calorimetry.

Figures 8 and 9 present heat source maps obtained for each jump in terms of heat source, which corresponds to the formation and propagation of PLC bands. For each jump, a set of three heat source maps is given. The three maps correspond, from the bottom to the top, to the beginning, the middle and maximum value of heat source during the jump. In order to distinguish the calorimetric signature of PLC bands, the maps given are anamorphosed, i.e. the scale is given in maximum and minimum values in the considered image. Here, PLC band kinematics is studied qualitatively, this is why no bar scale is shown.

Remark #4: the time constant has been determined from a thermal measurement at the specimen centre, where the thickness is the lowest (see Figure 1, A-A section). It should be noted that the time constant depends on the thickness (see Equation 4). As the value of heat source due to convection is two orders of magnitude less than that of total heat sources, this means that thickness variation does not affect the description of PLC band kinematics.

Several results can be derived from these maps:

- PLC bands are highly dissipative: they clearly appear in red color in the heat source field.
- PLC bands form a cross that propagates from the specimen centre to the borders of the square zone. The cross is formed in a zone under equibiaxial loading, and branches propagate in zones of different loading condition, *i.e.* from equibiaxial to quasi-uniaxial strain states. Further investigations of the effects of strain path on PLC kinematics are currently carried out in our laboratory.
- PLC band kinematics is highly repeatable from one heat source jump to another: the same shape of PLC bands and the same angles of the formed cross are observed.
- As thermoelasticity leads to low heat absorption compared to the heat produced by PLC bands, these maps can be assumed to give mechanical dissipation field. This assumption is classically used to neglect the effect of thermoelastic coupling (33; 38). Therefore, heat source maps can be considered as mechanical dissipation maps.

To investigate more precisely and quantitatively PLC band kinematics, Figure 10 focuses on the peak in the boxed zone. Four steps are sufficient to describe PLC band kinematics:

- Step I: by visualizing the movie provided as supplementary data, PLC bands always initiate close to the edges of the square zone and join the specimen centre to form a cruciform like pattern. In contrast to the specimen center, initiation zones are not submitted to an equibiaxial loading condition. By considering the kinetics of the formation of the cross, each cross branch can

be considered as independent from each other. Heat sources, *i.e.* dissipative waves, associated with PLC bands reach 1.08 $10^7 W/m^3$. At the specimen centre, heat sources are negative and reach -4.3 $10^6 W/m^3$. This means that, before the formation of the cross-shaped pattern, a large zone at the specimen centre deforms purely elastically. Elsewhere on the specimen surface, positive heat sources are obtained, meaning that plasticity occurs.

- Step II: PLC bands form a cross. The heat source is highest at the cross centre (approximately 3.9 $10^7 W/m^3$), and lowest in its branches (approximately 3 $10^7 W/m^3$). Elsewhere, the heat source is close to zero.
- Step III: PLC bands propagate in the loading direction (dotted lines in black color) with an angle close to 45° (48 and 42°), which forms a V-shaped pattern. The slight angular difference is probably due to material anisotropy. In addition, the centre of the square zone has the highest heat source level.
- Step IV: The PLC bands have disappeared and the heat source in the centre of the square zone is negative, meaning that this zone mostly deforms thermoelastically. Elsewhere, the heat source is positive and quite homogeneous, meaning that homogeneous plasticity occurs.

It should be noted that for the highest equivalent strain levels (superior to 30%), PLC band kinematics is no longer repeatable and symmetrical any more. As shown in Figure 9, only two branches of the cross develop in the same direction.

3.4.2 Remark on specimen failure

Figure **??** depicts the heat source field obtained just after a crack initiates at the centre of the square zone. The crack is boxed by the dotted line in white color. Its direction is the same as the one of PLC bands (48° with

the loading direction, in dotted line). At the crack tips, the heat source concentrations are exactly the same. A High heat source gradient is observed and the maximum heat source value is equal to 2.1 $10^9 W/m^3$, which is two orders of magnitude more than the heat source due to PLC bands. It should be noted that the highest heat source value is not exactly at the crack tip but behind it. Then, the crack propagates in the same direction until it reaches and goes through the square zone edges.

4 Conclusion

This paper provides the first study on spatio-temporal distribution of heat produced by PLC bands formed under equibiaxial tensile loading. Equibiaxial tensile testing has been carried out at an ambient temperature with an Al-Mg alloy. The temperature field was measured during the test and corresponding heat sources were reconstructed by means of the bidimensional formulation of the heat diffusion equation. The heat source map enables us to visualize spatio-temporal gradients in the calorific response of the material and to investigate the kinematics of PLC bands induced by equibiaxial tensile loading, which forms dissipative waves. At the specimen centre, the heat source exhibits jumps that fit well with jumps in the equivalent deformation rate and the temperature.

The results are a promising alternative of inquiry into the effects of complex loading conditions as those encountered during sheet metal forming processes on occurence and kinematics of PLC bands. Additionally, the present study provides additional data for the development and validation of PLC band kinematic models.

5 Funding Information

This work has received the financial support of the AIS Scientific Grant from Rennes Métropole (2012), the Mission of Resources and Skills Technology (MRCT) Grant from the French National Center for Scientific Research (2012), the Interdisciplinary Mission (MI) Grant from the French National Center for Scientific Research (2013).

References

[1] S. Nagarajan, R. Narayanaswamy, and V. Balasubramaniam. Study on the kinetics of thermomechanical response accompanying plastic instability in mild steel. *Mechanics of Materials*, 80, Part A:27 – 36, 2015.

[2] A Van Den Beukel. Theory of the effect of dynamic strain aging on mechanical properties. *Phys. Stat. Sol.*, 30:197, 1975.

[3] L. P. Kubin and Y. Estrin. *Acta metall*, 33:397, 1985.

[4] Y. Estrin, L.P. Kubin, and E.C. Aifantis. Introductory remarks to the viewpoint set on propagative plastic instabilities. *Scripta Metallurgica et Materialia*, 29(9):1147 – 1150, 1993.

[5] M. Zaiser and P. Hahner. Oscillatory modes of plastic deformation: Theoretical concepts. *Physica Status Solidi (b)*, 199(2):267–330, 1997.

[6] E. Rizzi and P. Hahner. On the portevin-le chatelier effect: theoretical modeling and numerical results. *International Journal of Plasticity*, 20(1):121 – 165, 2004.

[7] L. Casarotto, H. Dierke, R. Tutsch, and H. Neuhäuser. On nucleation and propagation of {PLC} bands in an Al-3Mg alloy. *Materials Science*

and Engineering: A, 527(12):132 – 140, 2009.

[8] H. Ait-Amokhtar, P. Vacher, and S. Boudrahem. Kinematics fields and spatial activity of portevin-le chatelier bands using the digital image correlation method. *Acta Materialia*, 54(16):4365 – 4371, 2006.

[9] H. Louche, K. Bouabdallah, P. Vacher, T. Coudert, and P. Balland. Kinematic fields and acoustic emission observations associated with the portevin le châtelier effect on an al–mg alloy. *Experimental Mechanics*, 48(6):741–751, 2008.

[10] Brindley B.J. and Worthington P.J. *Metall Rev*, 15:101, 1970.

[11] E. Pink and A. Grinberg. Serrated flow in a ferritic stainless steel. *Materials Science and Engineering*, 51(1):1–8, 1981.

[12] K. Chihab, Y. Estrin, L.P. Kubin, and J. Vergnol. The kinetics of the portevin-le chatelier bands in an al-5at%mg alloy. *Scripta Metallurgica*, 21(2):203 – 208, 1987.

[13] P. Hähner, A. Ziegenbein, E. Rizzi, and H. Neuhäuser. Spatiotemporal analysis of portevin-le châtelier deformation bands: Theory, simulation, and experiment. *Phys. Rev. B*, 65:134109, 2002.

[14] H. Jiang, Q. Zhang, X. Chen, Z. Chen, Z. Jiang, X. Wu, and J. Fan. Three types of portevin-le chatelier effects: Experiment and modelling. *Acta Materialia*, 55(7):2219 – 2228, 2007.

[15] T.A. Lebedkina and M.A. Lebyodkin. Effect of deformation geometry on the intermittent plastic flow associated with the portevin-le chatelier effect. *Acta Materialia*, 56(19):5567 – 5574, 2008.

[16] J. Coër, P.Y. Manach, H. Laurent, M.C. Oliveira, and L.F. Menezes. Piobert-Lüders plateau and Portevin-Le Chatelier effect in an al-mg alloy in simple shear. *Mechanics Research Communications*, 48:1–7, 2013.

[17] J. Balik and P. Lukac. Portevin-Le Chatelier instabilities in al-3 mg conditioned by strain rate and strain. *Acta Metallurgica et Materialia*, 41(5):1447 – 1454, 1993.

[18] H Fujita and T Tabata. The effect of grain size and deformation substructure on mechanical properties of polycrystalline aluminum. *Acta Metallurgica*, 21(4):355 – 365, 1973.

[19] A. Korbel and H. Dybiec. The problem of the negative strain-rate sensitivity of metals under the Portevin-Le Chatelier deformation conditions. *Acta Metallurgica*, 29(1):89 – 93, 1981.

[20] A.T Thomas. The tensile deformation behaviour of an aluminium-magnesium alloy. *Acta Metallurgica*, 14(10):1363 – 1374, 1966.

[21] M. Li and DJ Lege. Serrated flow and surface markings in aluminum alloys. *J. Eng. Mater. Technol.*, 120:48–56, 1998.

[22] J. Coër, C. Bernard, H. Laurent, A. Andrade-Campos, and S. Thuillier. The effect of temperature on anisotropy properties of an aluminium alloy. *Experimental Mechanics*, 51(7):1185–1195, 2010.

[23] Q. Hu, Q. Zhang, P. Cao, and S. Fu. Thermal analyses and simulations of the type a and type b portevin-le chatelier effects in an almg alloy. *Acta Materialia*, 60(4):1647 – 1657, 2012.

[24] H. Ait-Amokhtar, C. Fressengeas, and S. Boudrahem. The dynamics of Portevin-Le Chatelier bands in an almg alloy from infrared thermography. *Materials Science and Engineering: A*, 488:540 – 546, 2008.

[25] C. Bernard, J. Coër, H. Laurent, P. Chauvelon, and P. Y. Manach. Relationship between local strain jumps and temperature bursts due to the Portevin-Le Chatelier effect in an al-mg alloy. *Experimental Mechanics*, 53(6):1025–1032, 2013.

[26] M.P. Moutrille, X. Balandraud, M. Grédiac, K. Derrien, and D. Bap-

tiste. Applying thermoelasticity to study stress relief and crack propagation in aluminium specimens patched with composite material. *J. Strain Anal. Eng. Des.*, 28:423–433, 2008.

[27] J. R. Samaca Martinez, J.-B. Le Cam, X. Balandraud, E. Toussaint, and J. Caillard. Thermal and calorimetric effects accompanying the deformation of natural rubber. part 1: Thermal characterization. *Polymer*, 54:2717 – 2726, 2013.

[28] D. Delpueyo, X. Balandraud, and M. Grédiac. Applying infrared thermography to analyse martensitic microstructures in a Cu-Al-Be shape-memory alloy subjected to a cyclic loading. *Materials Science and Engineering: A*, 528(28):8249 – 8258, 2011.

[29] X. Feng, G. Fischer, R. Zielke, B. Svendsen, and W. Tillmann. Investigation of {PLC} band nucleation in {AA5754}. *Materials Science and Engineering: A*, 539:205 – 210, 2012.

[30] C. Badulescu, M. Grédiac, H. Haddadi, J.-D. Mathias, X. Balandraud, and H.-S. Tran. Applying the grid method and infrared thermography to investigate plastic deformation in aluminium multicrystal. *Mechanics of Materials*, 43(1):36 – 53, 2011.

[31] A.E. Morabito, A. Chrysochoos, V. Dattoma, and U. Galietti. Analysis of heat sources accompanying the fatigue of 2024 {T3} aluminium alloys. *International Journal of Fatigue*, 29(5):977 – 984, 2007.

[32] J.R. Samaca Martinez, J.-B. Le Cam, X. Balandraud, E.Toussaint, and J. Caillard. New elements concerning the mullins effect: A thermomechanical analysis. *European Polymer Journal*, 55:98–107, 2014.

[33] A. Chrysochoos and H. Louche. Thermal and dissipative effects accompanying luders band propagation. *Mat Sci Eng A-struct*, 307:15–22, 2001.

[34] B. Berthel, B. Wattrisse, A. Chrysochoos, and A. Galtier. Thermographic analysis of fatigue dissipation properties of steel sheets. *Strains*, 43:273–279, 2007.

[35] B. Wattrisse, A. Chrysochoos, J.-M. Muracciole, and M. Nmoz-Gaillard. Analysis of strain localization during tensile tests by digital image correlation. *Experimental Mechanics*, 41:2939, 2001.

[36] A. Chrysochoos, V. Huon, F. Jourdan, J.-M. Muracciole, R. Peyroux, and B. Wattrisse. Use of full-field digital image correlation and infrared thermography measurements for the thermomechanical analysis of material behaviour. *Strain*, 46:117–130, 2010.

[37] H. Louche, P. Vacher, and R. Arrieux. Thermal observations associated with the portevin-le chatelier effect in an al-mg alloy. *Materials Science and Engineering: A*, 404:188 – 196, 2005.

[38] D. Delpueyo, X. Balandraud, and M. Grediac. Calorimetric signature of the Portevin-Le Chatelier effect in an aluminum alloy from infrared thermography measurements and heat source reconstruction. *Materials Science and Engineering: A*, 651:135 – 145, 2016.

[39] T.A. Prater and H.J. Read. The strength and ductility of electrodeposited metals - the hydraulic bulge test. *Plating*, 36:1221, 1949.

[40] T. D. Dudderar, F. B. Koch, and E. M. Doerries. Measurement of the shapes of foil bulge-test samples. *Experimental Mechanics*, 17(4):133–140, 1977.

[41] I Zidane, D Guines, L Léotoing, and E Ragneau. Development of an in-plane biaxial test for forming limit curve (flc) characterization of metallic sheets. *Measurement Science and Technology*, 21(5):055701, 2010.

[42] S. Zhang, L. Leotoing, D. Guines, and S. Thuillier. Potential of the

Cross Biaxial Test for Anisotropy Characterization Based on Heterogeneous Strain Field. *Experimental Mechanics*, 55(5):817–835, 2015.

[43] Wei Liu, Dominique Guines, Lionel Leotoing, and Eric Ragneau. Identification of sheet metal hardening for large strains with an in-plane biaxial tensile test and a dedicated cross specimen. *International Journal of Mechanical Sciences*, 101:387–398, 2015.

[44] Q.S. Nguyen, P. Germain, and P. Suquet. Continuum thermodynamics. *J Appl Sci*, 50:1010–1020, 1983.

[45] T. Boulanger, A. Chrysochoos, C. Mabru, and A. Galtier. Calorimetric analysis of dissipative and thermoelastic effects associated with the fatigue behavior of steels. *International Journal of Fatigue*, 26:221–229, 2007.

[46] A. Chrysochoos and H. Louche. An infrared image processing to analyse the calorific effects accompanying strain localisation. *Int J Eng Sci*, 38:1759–1788, 2000.

Table 1

Ratio of heat diffusion over total source for each temperature drop number

Number of temperature drop in Fig. 4	1	2	3	4	5
$\frac{\lvert\rho\ C_{E,V_k}\ \left(\frac{\theta+T_0-T_{amb}}{\tau}\right)-k(\Delta_{2D}\theta)\rvert}{\lvert\rho\ C_{E,V_k}\dot{\theta}\rvert}\times 100$	0.5%	0.3%	0.3%	0.4%	0.8%

A Supplementary data

Supplementary data associated with this paper can be found in the online version.

Figure 1: Specimen geometry

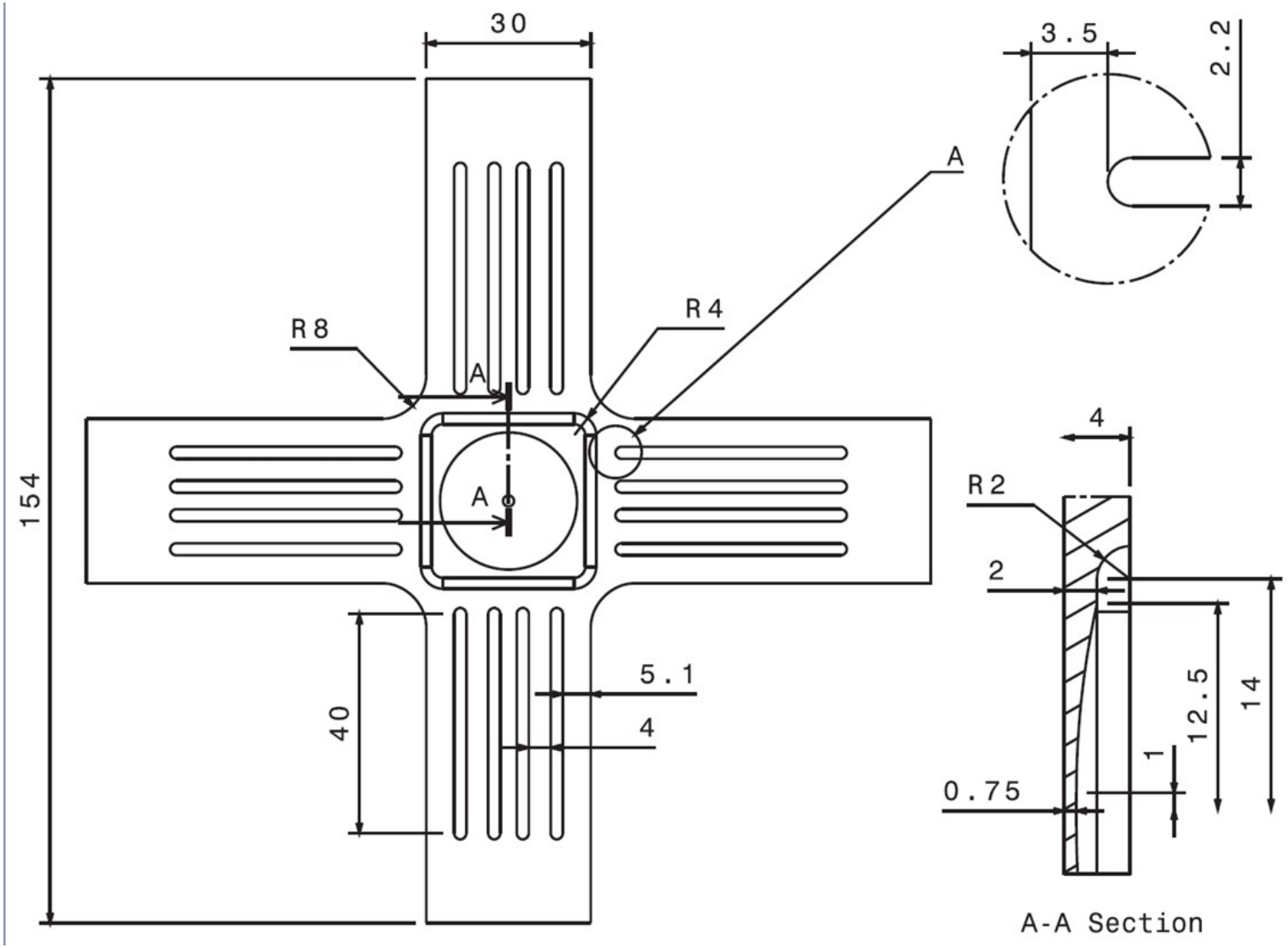

Figure 2(a): Overview of the experimental set up

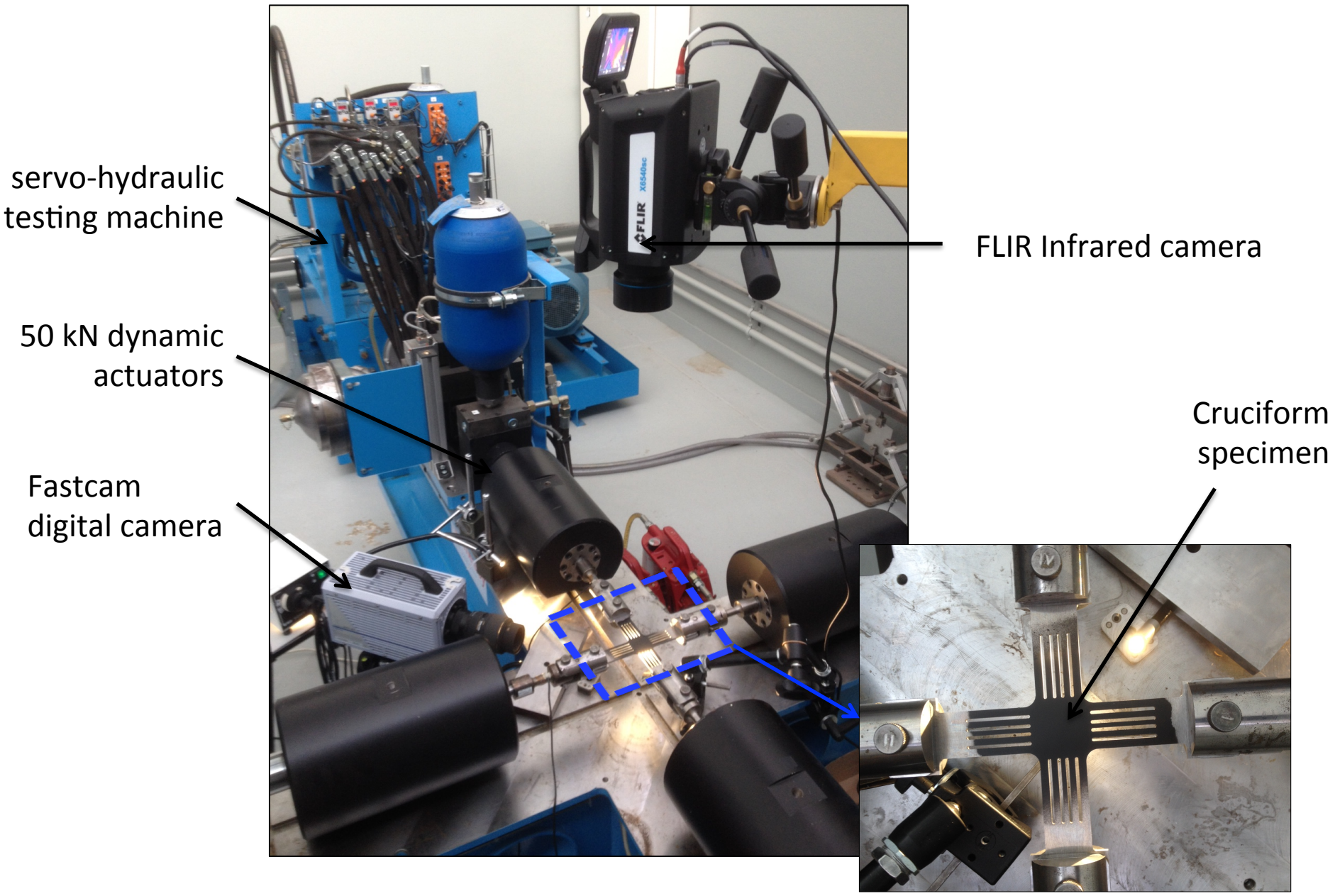

Figure 2(b): Zones observed by the two cameras

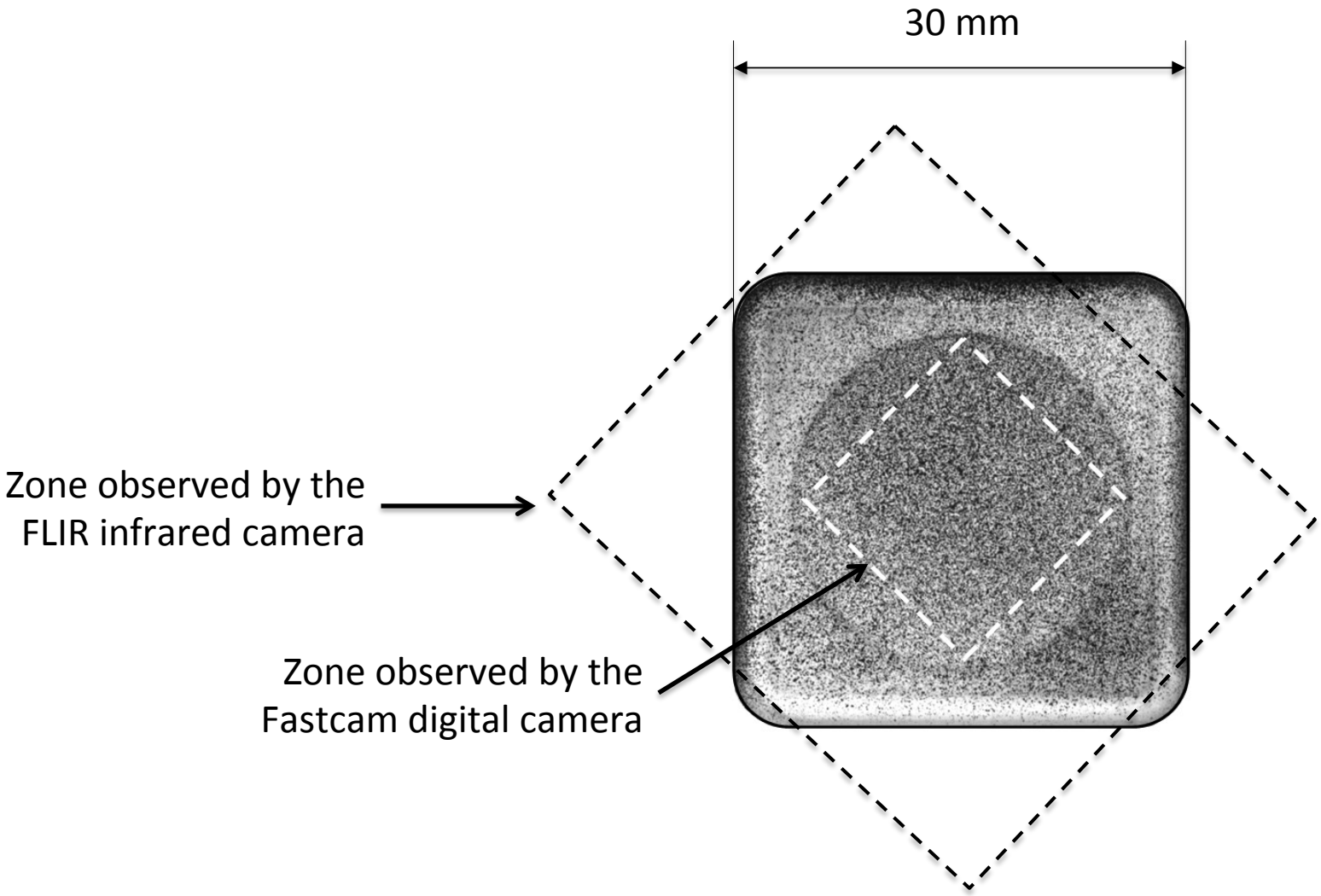

Figure 3: Force versus time in the two directions

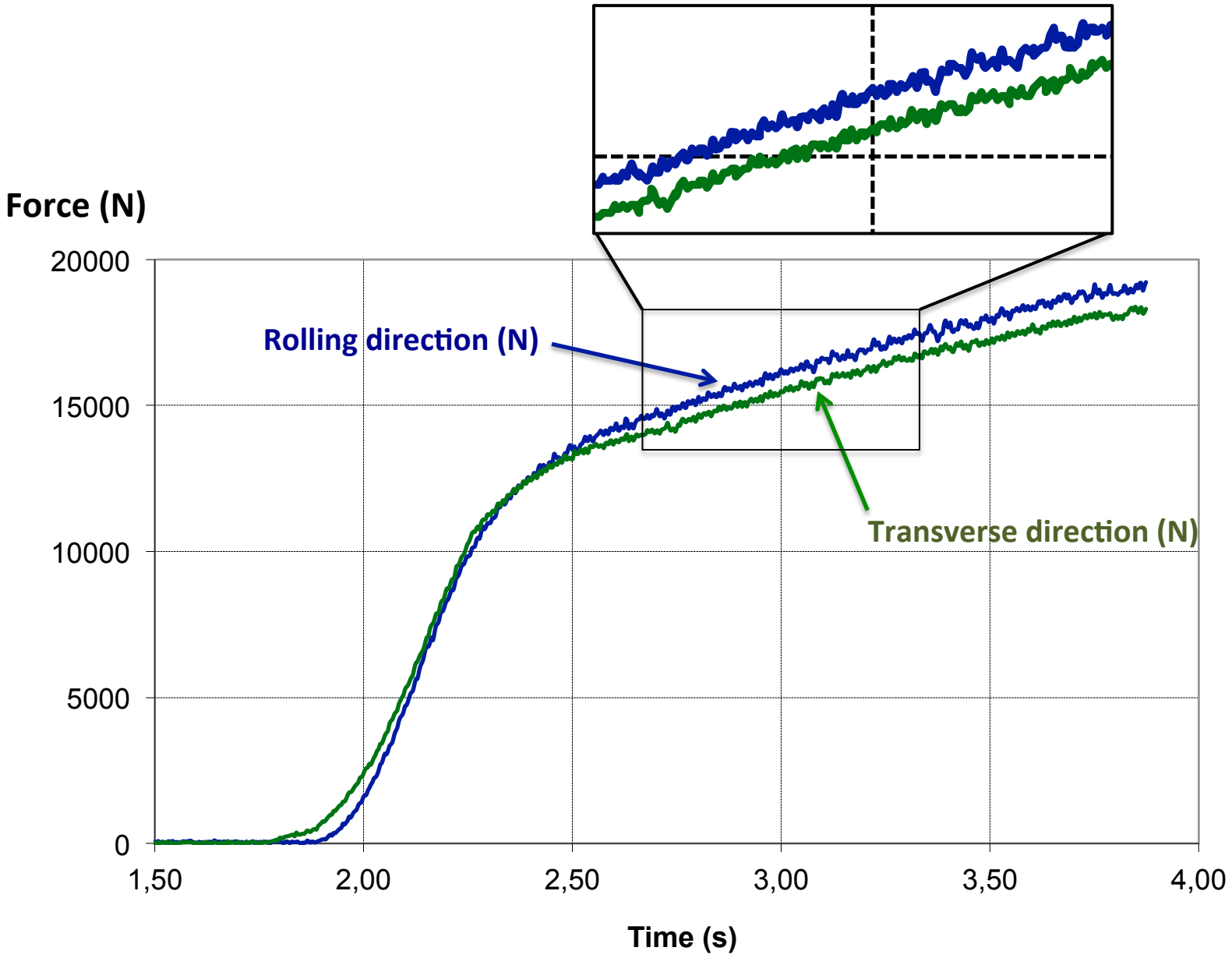

Figure 4: Effects of PLC bands on equivalent strain and temperature variations.

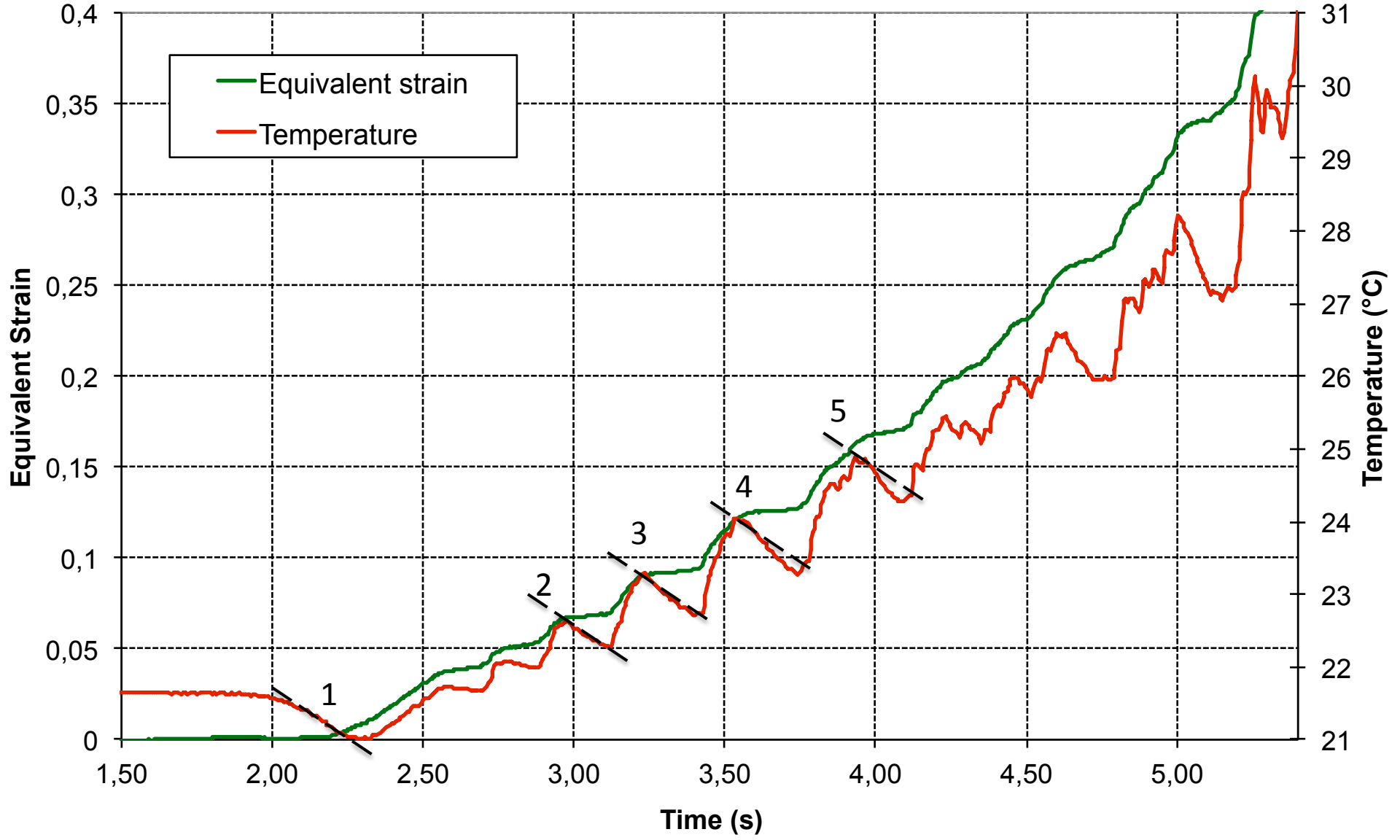

Figure 5: Temperature and heat sources variations during the loading

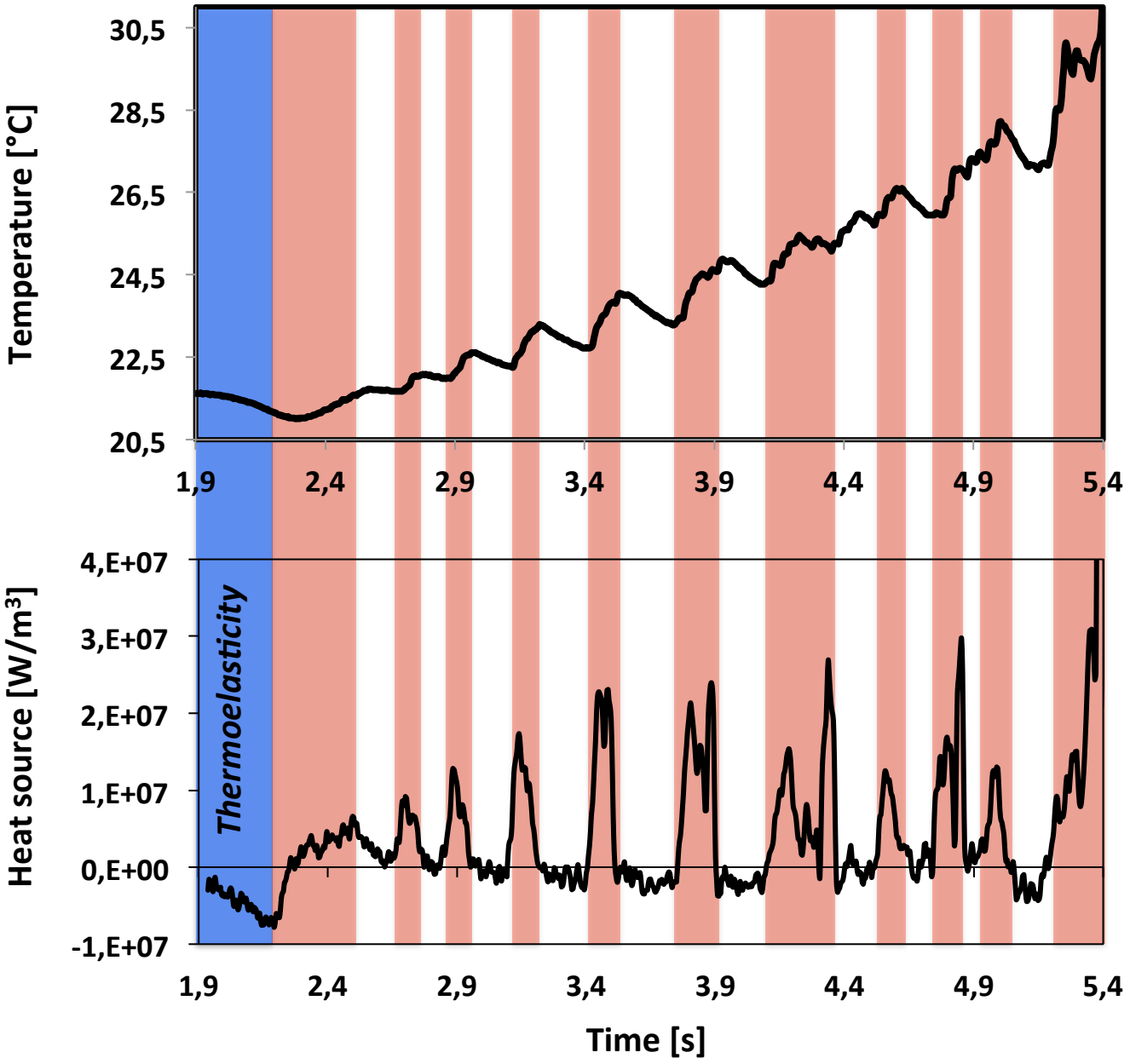

Figure 6: heat source and equivalent deformation rate

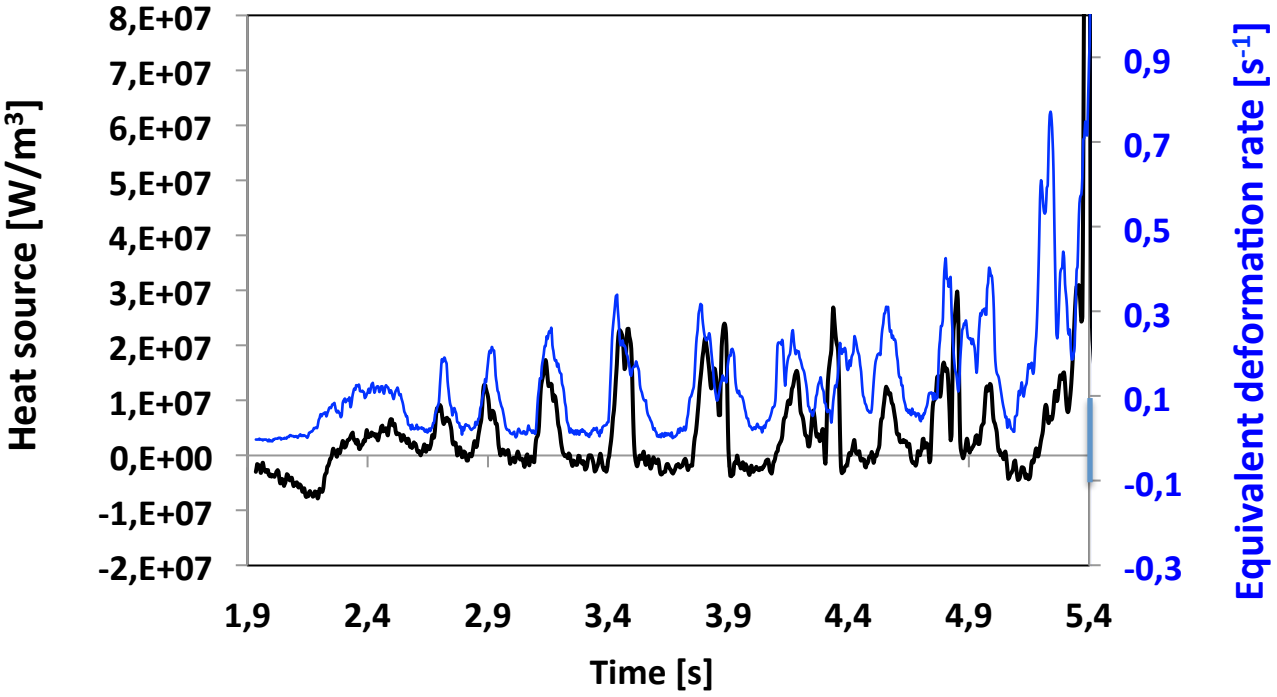

Figure 7: Relative contribution of conduction and convection to the heat sources

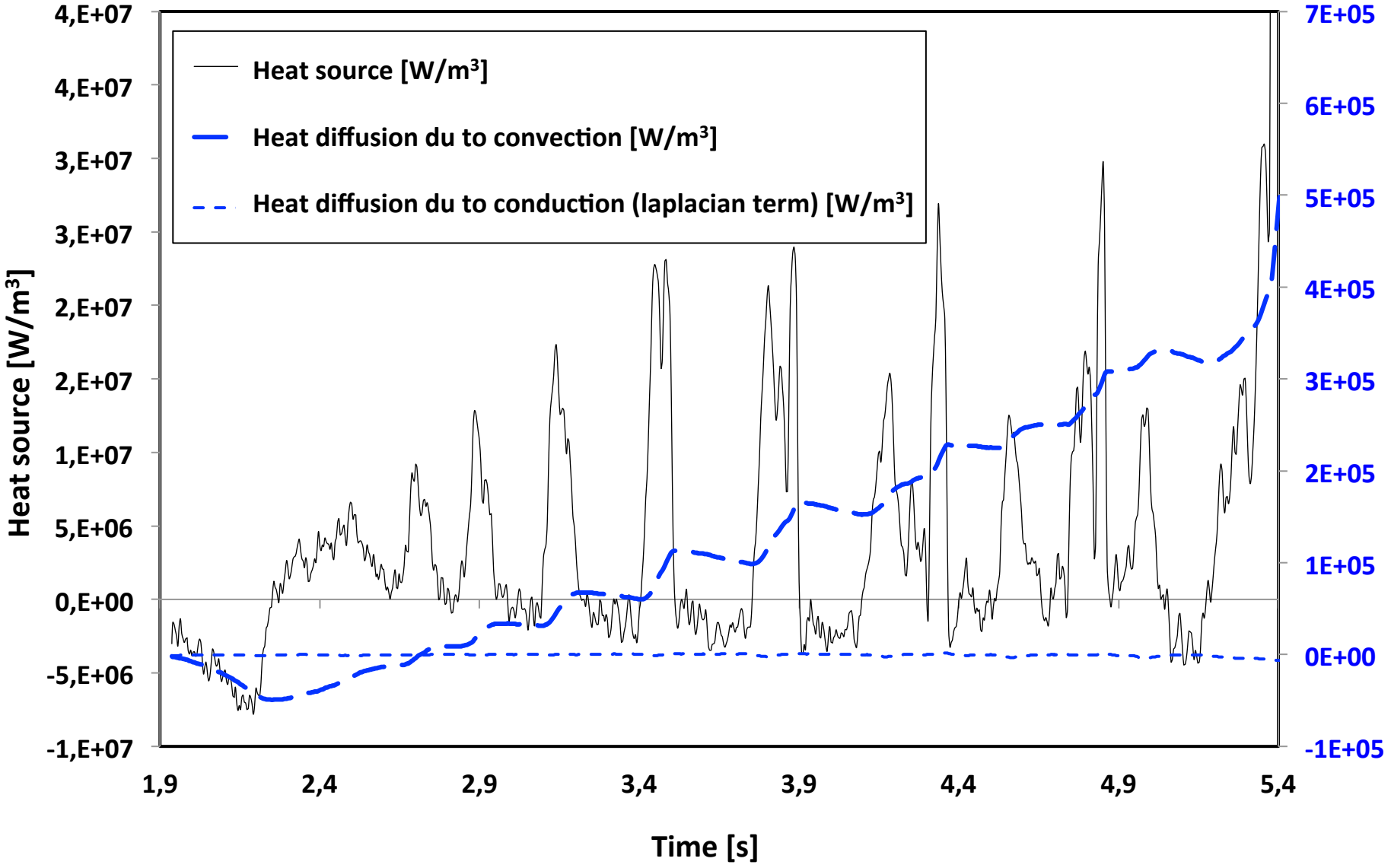

Figure 8: heat source maps highlight that the PLC band kinematic is the same. A double PLC band network is observed, especially at the highest strains

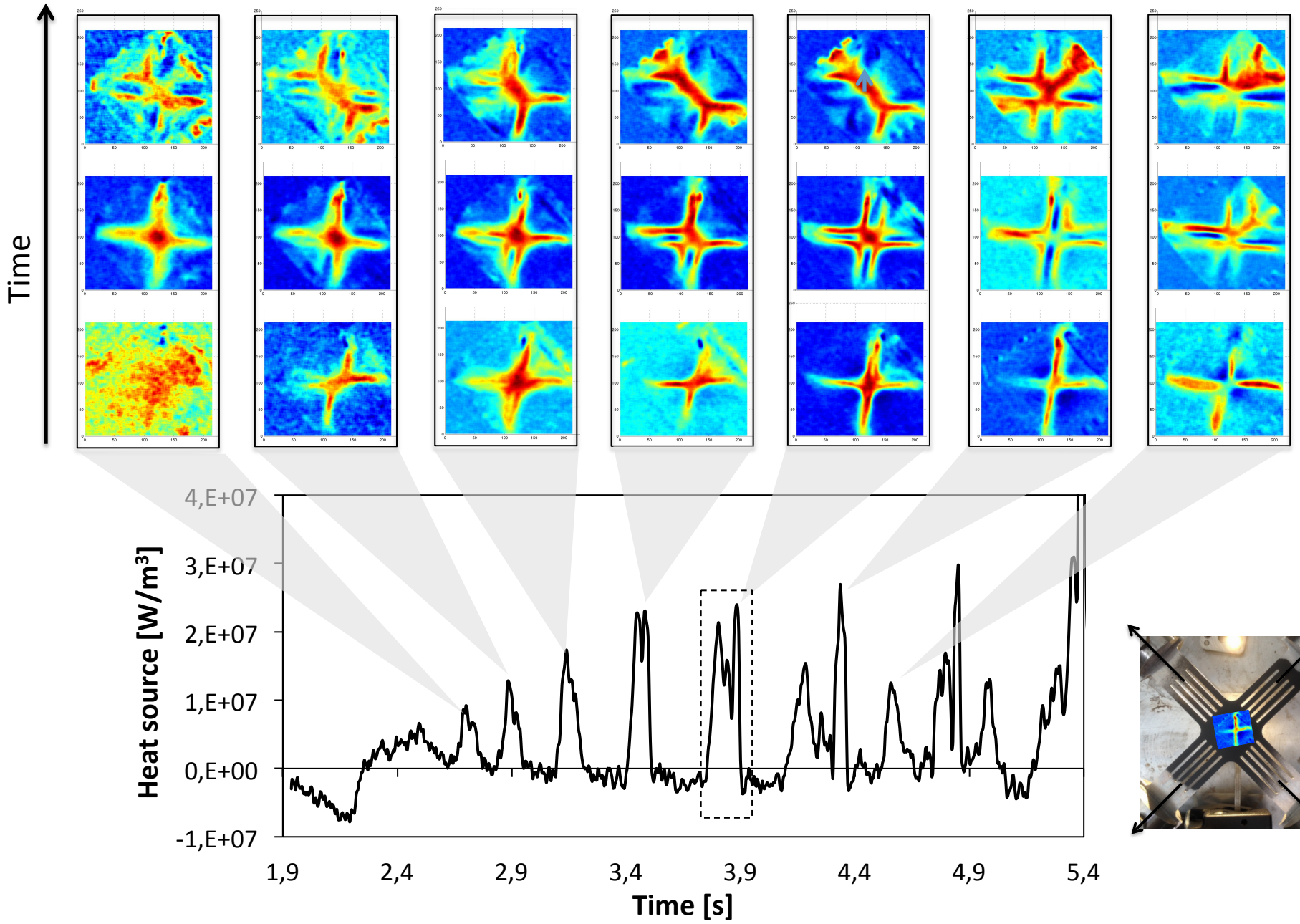

Figure 9: heat source maps before specimen failure. PLC bands propagate in a given direction, not in two perpendicular directions as for lower strain level.

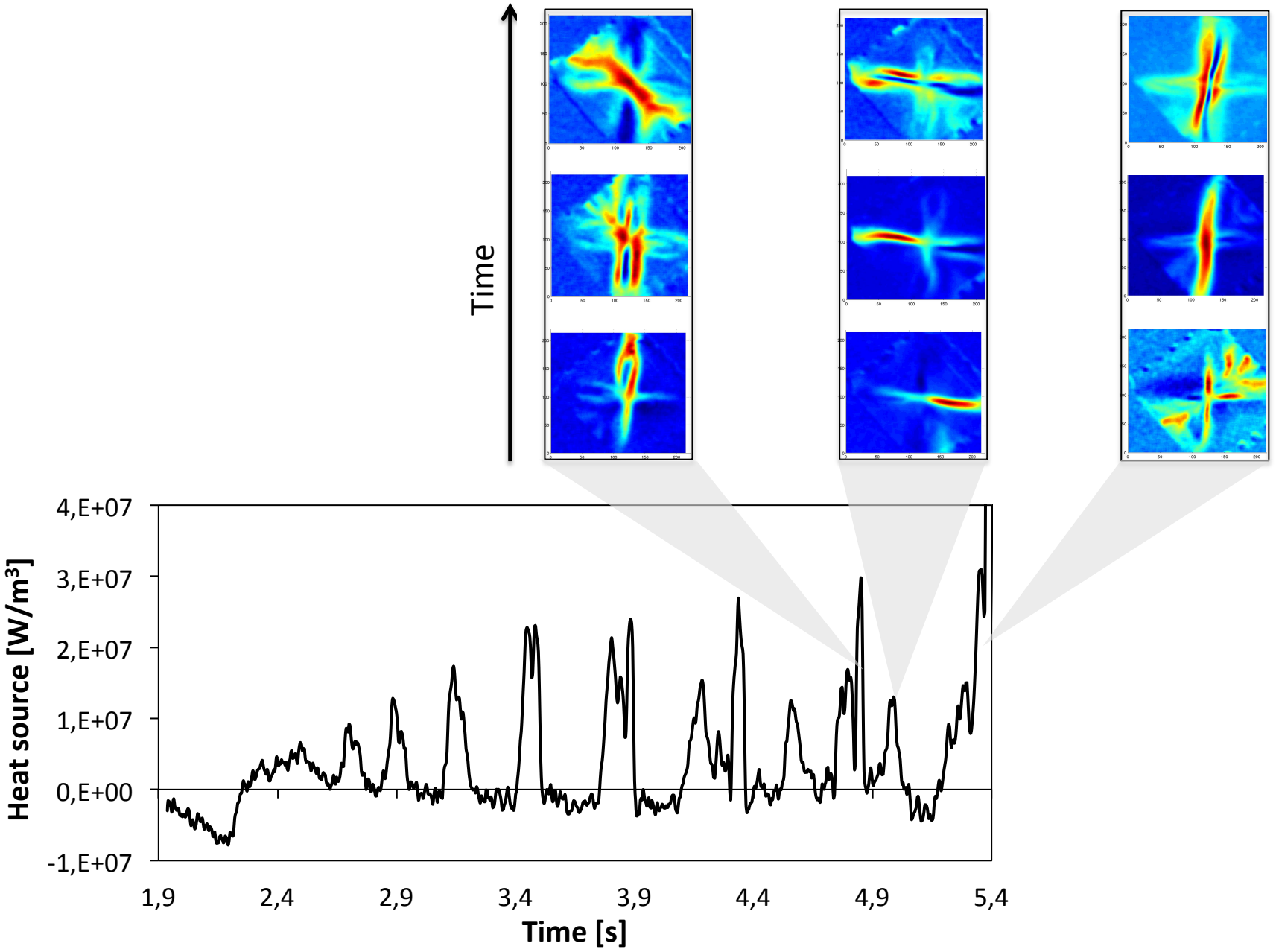

Figure 10: Initiation and propagation path of PLC band (dotted lines in black color)

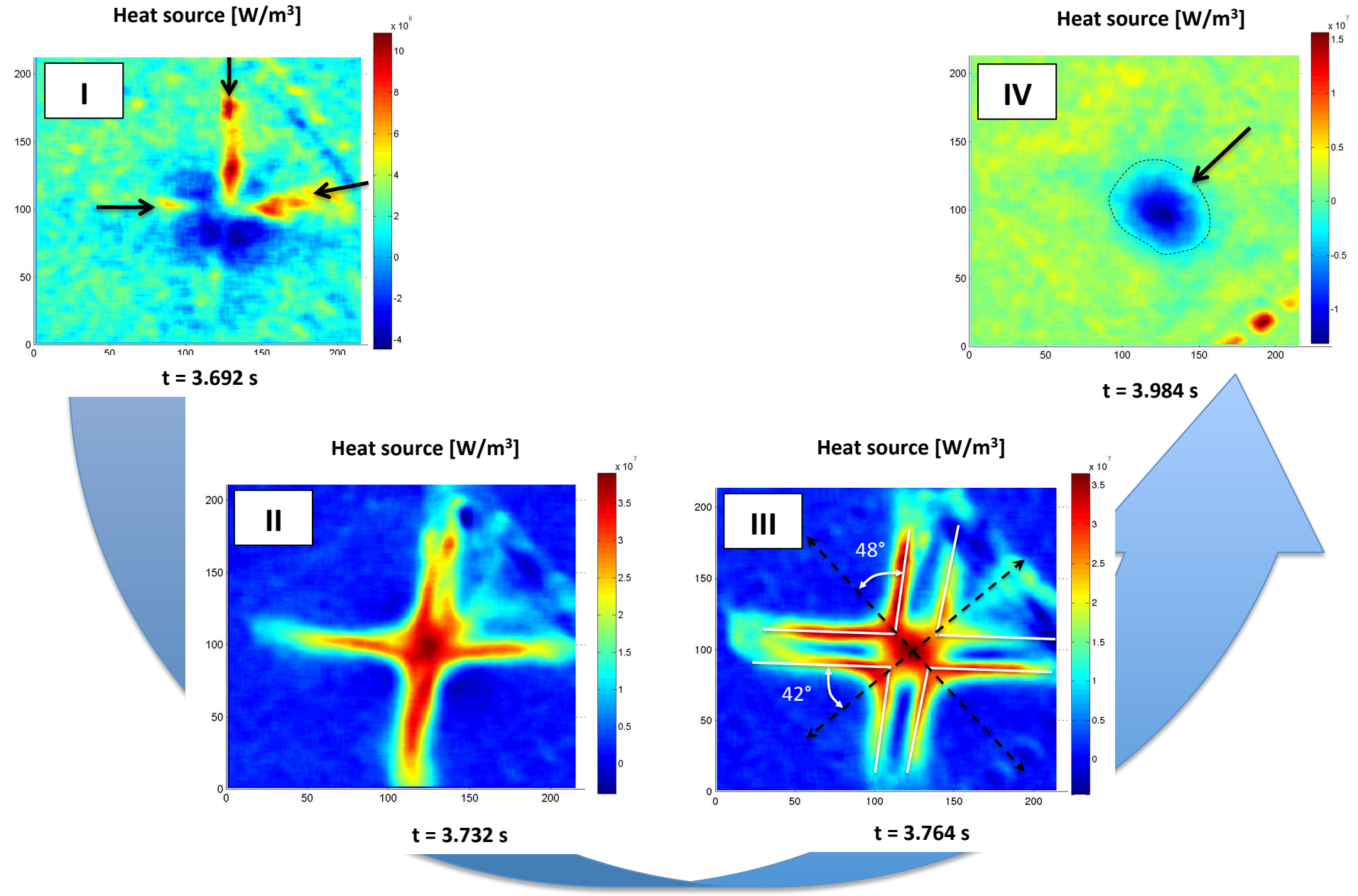

Figure 11: Heat source map after a crack initiates